



Nanomaterials in Proton Exchange Membrane Fuel Cells

7

Yufeng Zhang, Rui Xue, Weijian Yuan, and Xiaowei Liu

Contents

7.1	Introduction	200
7.2	Carbon Nanotubes (CNT) Used in Direct Methanol Fuel Cells (DMFCs)	202
7.3	Graphene Applied in Direct Methanol Fuel Cells (DMFCs)	207
7.3.1	Graphene Used as Barrier Layer	207
7.3.2	Graphene Used in Catalyst	209
7.4	Other Nanomaterials Applied in PEMFC	218
7.4.1	Zero-Dimensional Nanomaterials	218
7.4.2	One-Dimensional Nanomaterials	219
7.4.3	Two-Dimensional Nanomaterials	219
7.4.4	Three-Dimensional Nanomaterials	220
7.5	Conclusion	221
	References	221

Abstract

With the rapid development of modern science and technology in the current society, environmental conservation and taking advantage of new energy sources have become the core strategies of sustainable development for society. Micro-energy technology has boasted a huge potential in market demand and attracted a great deal of interest in research and development since it is safe, efficient, and

Author Contributions

Weijian Yuan is responsible for the part of “Graphene Used in Catalyst” and “Other Nanomaterials Applied in PEMFC.” Rui Xue is responsible for the part of “CNT Used in Catalyst” and “Graphene Used as Barrier Layer.” Yufeng Zhang and Xiaowei Liu are in charge of the design, modification, and validation of the whole manuscript.

Y. Zhang (✉) · R. Xue · W. Yuan · X. Liu
MEMS Center, Harbin Institute of Technology, Harbin, China
e-mail: yufeng_zhang@hit.edu.cn

environmentally friendly and meets the goals for portable devices on the exterior, weight, and endurance. Although significant advancements have been achieved for proton exchange membrane fuel cells (PEMFCs) in recent years, PEMFCs still suffer from the key problems of low power density and fuel utilization, which are related, respectively, to poor reaction kinetics and methanol permeation through the membrane (*viz.*, methanol crossover). Nanomaterials recently have attracted lots of attention owing to their distinguishing physical and chemical characteristics. Among them, carbon-based nanostructured materials such as graphene (G) and carbon nanotube (CNTs) have been successfully applied in fuel cells. PEMFC combined with nanostructured materials has remarkable improvements compared with the traditional fuel cells.

7.1 Introduction

The increase in population and migration of individuals forming large metropolitan population centers requires a vast infrastructure to accommodate, transport, and feed. This necessitates the use of energy in the form of fossil fuels from the industrial revolution that caused an increase in carbon dioxide emission and potential global warming. The current approach is to lessen energy production from fossil fuels using alternative energy resources such as fuel cells, which convert chemical energy to electrical energy with zero or near-zero emission of harmful gases. With the rapid development and increasing market demand for micro-power sources, direct methanol fuel cell (DMFC) based on microelectromechanical system (MEMS) technology is currently becoming the research hotspot due to its great application prospect in the future. The DMFC has drawn significant attention due to its advantages such as eco-friendly, efficiency, high energy density, abundant reserves, and convenient for storage and transport [1–5].

The basic structure of DMFC is shown in Fig. 7.1 (from Yuan et al., with permission License 4153521292378 [6]), mainly composed of the anode plate, the membrane electrode assembly (MEA), and cathode plates. The MEA is made up of the diffusion layer (DL), catalyst, and proton exchange membrane (PEM). The anode plate of the flow field structure is mainly used to support the DL, distribute reactants, and collect current. The diffusion layers serve three purposes, as a gas, liquid, and electron channels, which are mainly used as a support for the catalytic layer, a collection of electrons, and the conduction of reactants and products. The catalytic layer provides a place for electrochemical reaction. The PEM as a key component in MEA serves as a proton conduction and separates the fuel and oxidant at the same time. In the anode reaction of DMFC, methanol solution flow field reaches the catalytic layer through the anode diffusion layer by convection and diffusion. Under the effect of catalyst particles, an oxidation reaction occurs, generating carbon dioxide (CO_2) gas and releasing hydrogen protons (H^+) and electron (\bar{e}) simultaneously. The CO_2 gas returns to the anode flow channel through the diffusion layer and ultimately discharges with the methanol solution flow. Meanwhile, the

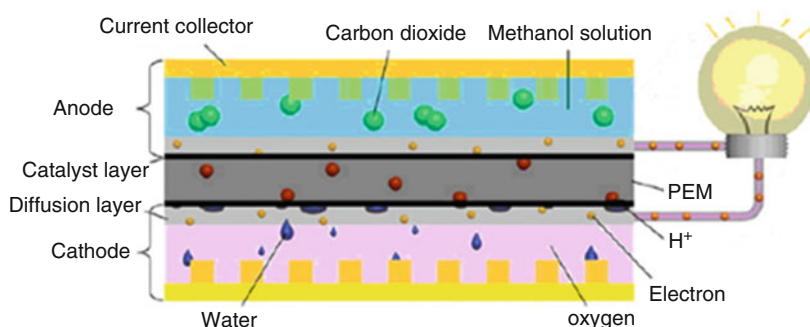
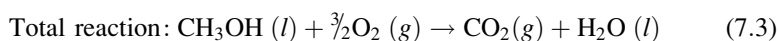
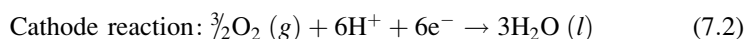
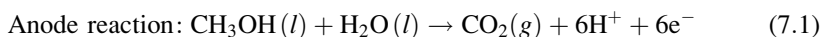


Fig. 7.1 Schematic of the basic structure of a DMFC [6]

electrons transfer from the anode compartment through the external circuit to the cathode compartment, generating direct electricity. The protons (H^+) directly diffuse to the surface of the cathode catalyst layer through the PEM. These protons will react with oxygen, which transports through the diffusion layer to the surface of the cathode catalyst layer. The electrochemical reaction will result in H_2O production. Detailed chemical reaction Eqs. (7.1), (7.2), and (7.3) are shown as follows:



However, the key challenges for the intensive research on DMFC lie in the enhancement of DMFC performance. Current FC performance is suboptimal even with laboratory-based stacks, whose performance rapidly deteriorates in real FC industrial applications. There are a number of reasons for this suboptimal performance. One of the disadvantages is cathode flooding related to water management. After the water molecules on the surface of the cathode catalyst layer are generated, the molecule migrates through the diffusion layer into the cathode flow channel; however, if the gas flow rate is too low, some quantity of water molecules cannot be efficiently discharged into the air, causing flooding. The cathode water-flooding phenomenon will block both porosities of the porous diffusion layer and cathode flow channel. This blocking will cause a serious impediment to oxygen transport, and as a result, a shortage of the cathode gas supply will occur that, in turn, will lead to an increase in polarization, lowering FC performance. Therefore, the water generated in the cathode compartment should be discharged as quickly as possible. But at the same time, the PEM should contain water content, in order to mitigate mass transfer resistance. The DMFC cathode water management is a complex process, which is one of the key factors in limiting FC performance. One method to decrease cathode flooding is an introduction of high-speed airflow, which allows

water to flow at increased velocities. This area of research can be tailored toward design and construction of air-breathing DMFCs. To solve the key components of the material and structure design, researchers must focus on the development of nanostructured materials [7–14].

Methanol crossover is a second key problem hindering the development of DMFC. In the internal DMFC, part of methanol molecules which was not involved in the electrochemical reaction transmit through the PEM from the anode directly to the cathode. This phenomenon is called the methanol crossover. (1) Methanol crossover can cause degradation of DMFC performance, which mainly results from oxidizing reaction of methanol molecules penetrating to the cathode that will produce a mixed over potential, reducing the working voltage of DMFC; and (2) methanol crossover is a waste of fuel, and produces excess heat, which also degrades FC performance [15–19].

Low catalyst activity is the third technical DMFC obstacle especially under the condition of low temperature. Herein, anodic oxidation catalyst activity needs to be improved for optimal FC performance. If the anode catalyst activity increases, the methanol consumption will also be increased; on the other hand, osmotic quantity will be decreased. This process will also reduce the negative effect of methanol crossover, improving FC performance.

With the increased development of nanometer-sized materials in recent years, miniature DMFCs based on nanomaterials have received great attention. The nanostructured materials used in DMFC include carbon nanotube paper (i.e., Bucky paper), carbon nanotube (CNT) film, graphene (G) aerogels and hydrogel, etc.. Considering the nanostructure material, graphene which has an excellent physical and chemical performance and stability is a suitable material for DMFC-based catalyst.

7.2 Carbon Nanotubes (CNT) Used in Direct Methanol Fuel Cells (DMFCs)

In an MEA, the gas diffusion layer has two major functions. First, the microporous structure allows the reactants in the diffusion layer to spread into the catalyst layer. Here, the reactants can also uniformly disperse on the catalytic layer, which provides the effective area of the electrochemical reaction, and the layer arrangement gives the highest surface area. The second function is to export the electrons from the anode electrochemical reaction generated by the external circuit and import electrons from open circuit potential (OCP) into the catalyst layer. Therefore, the selection of gas diffusion layer material must be able to provide a conduction and is an important consideration.

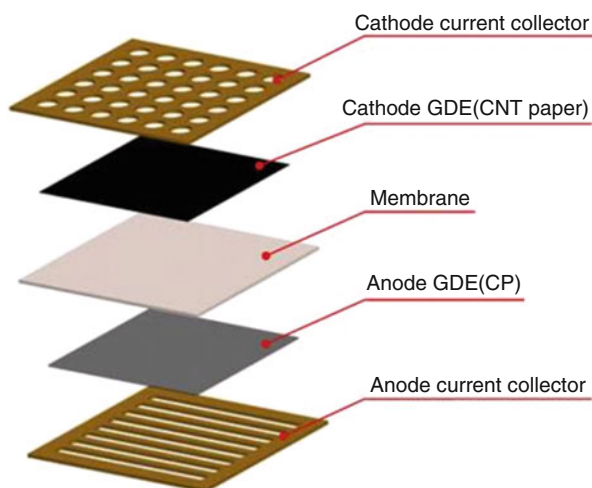
A novel MEA structure of DMFC controls water management and decreases methanol crossover. The CNT paper replacing carbon paper (CP) as a gas diffusion layer (GDL) enhances water back diffusion which passively prevents flooding in the cathode and promotes low methanol crossover [20]. Generally, porous materials such as CP or carbon cloth are chosen as components of the GDL. The FC produces

water during operation, as working FC temperatures are below the boiling point of water, so water always exists in liquid form in the compartment. When large amounts of water are stored around the electrodes, the water-flooding phenomenon causes increased oxygen mass transfer resistance and serious cathode polarization, leading to a rapid decrease in FC performance. So as the GDL, CP or carbon cloth must be of a certain hydrophobicity, and the general processing is to add polytetrafluoroethylene (PTFE) in carbon paper to improve the GDL paper hydrophobicity [21].

In this work, the water transmittal layer is CNT paper made from an aggregate of CNTs. The CNTs are allotropes of carbon with a cylindrical nanostructure which is supplied by Suzhou Creative-Carbon Nanotechnology Co. Ltd., China. For purification and chemical modification, the multi-walled carbon nanotubes (MWNTs) are dispersed into concentrated sulfuric acid (98%) and concentrated nitric acid (70%) mixture solution of 3:1 v/v by ultrasonication for 8 h. The mixture solution is diluted by large quantities of water to remove acid and filtered by polyvinylidene fluoride (PVDF) membrane. After chemical modification, the MWNTs have oxygenated functional groups which make MWNTs hydrophilic, and the wetting angle is 73.5°. The mixture of 100 mg of purified MWNT and 1 g Triton X-100 (a surfactant) was dispersed into 100 mL of deionized water by ultrasonication for 2.5 h [22]. The as-prepared MWNT suspension was filtered through the wetted PVDF membrane by a positive nitrogen gas pressure of 500 kPa to produce a well-known Bucky paper. Due to the van der Waals forces, the interaction of CNT surface and surfactant can be strong and stable. Subsequently, the produced Bucky paper is flushed in an effective solvent (2:1 v/v, water to methanol) to remove residual Triton X-100 surfactant after being rinsed by deionized water. Afterward, the produced Bucky paper is dried in a vacuum oven for 5 h and then peeled off from the PVDF membrane. The thickness of the CNT papers is controlled by the concentration of the MWNT suspension. Finally, the CNT paper is cut into 10 × 10 mm as a water transmittal layer. A piece of five-layered MEA with an active area of 10 × 10 mm is fabricated in a self-breathing DMFC by the catalyst-coated membrane (CCM) and hot press method. The hydrophilic catalyst layer is prepared to utilize the decal transfer method to form the CCM, with an anode catalyst layer of platinum-ruthenium (Pt-Ru) black (4.0 mg·cm²) and a cathode catalyst layer of Pt black (2.0 mg·cm²) and a Nafion 117 membrane between them. Then, for forming the GDL, CP (TGPH-090, Toray Inc.) is prepared by the hydrophobic (10 wt. % PTFE for the anode and 30 wt. % PTFE for the cathode, respectively) and pore-formed (ammonium hydrogen carbonate, NH₄HCO₃) pretreatment. Finally, the CCM is sandwiched between two GDLs and hot-pressed under the condition of 130 °C and 4 MPa for 120 s. The CNT is embedded between the five-layered MEA and cathode current collector which serves as a collector and distributor layer of water and electron as shown in Fig. 7.2. Figure 7.2 is from Deng et al., with permission License 4153540257896 [20].

Stainless steel plates with a thickness of 300 μm are chosen to fabricate the anode and cathode current collectors, and the structure of anode and cathode is fabricated by MEMS technology. A 500 nm layer of gold (Au) is deposited on the current collectors by the magnetron sputtering ion plating (MSIP) to reduce contact

Fig. 7.2 The CNT embedded between the five-layered MEA and cathode current collector [21]



resistance and avoid chemical corrosion. A CNT paper with a thickness of 150 μm is utilized to absorb water from the cathode which keeps MEA in a proper hydration and prevent cathode flooding. From the SEM image of CNT paper shown in Fig. 7.3 (from Deng et al., with permission License 4153540257896) [20], we can see that the CNT paper contains a high porous ratio structure which causes it to have a capillary phenomenon, and the high porous ratio structure also makes the oxygen diffuse through CNT expediently. The CNT paper is hot-pressed on the cathode side of MEA at 130 $^{\circ}\text{C}$ and 4 MPa for 120 s to form the CNT-MEA compound structure.

As the radius of self-breathing openings on the cathode current collector is very small, long-term operation of the self-breathing DMFC will cause cathode flooding easier than conventional designs. In order to determine the flooding behavior of DMFC with and without CNT-MEA which uses the CNT paper as water transmittal layer, a short-term voltage assessment with 3 M methanol solution and flow rates of 1 mL/min was conducted at ambient conditions. A measurement comparison of cell potential as a function of time between the DMFC without and with CNT as the water transmittal layer is summarized in Fig. 7.4 (from Deng et al., with permission License 4153540906158) [21].

The output voltage versus time measurements is recorded for 2000 s at a current of 120 mA. It can be seen that the voltage of the DMFC composed of CP-MEA is higher than that of DMFC composed of CNT-MEA during the first 150 s. After this time point, the voltage of DMFC composed of CNT-MEA constantly increases and exceeds that of DMFC composed of CP-MEA. It was also found the voltage of DMFC composed of CP-MEA decreases at 430 s of operation and then improves. The performance of DMFC composed of CNT-MEA is inferior to that of the DMFC composed of CP-MEA at the beginning of operation because oxygen needs time to diffuse through the CNT layer which leads to an oxygen starvation for a short time period. At the same time, the DMFC composed of CP-MEA is flooded, leading to voltage declination and then voltage inclination after 430 s due to DMFC which

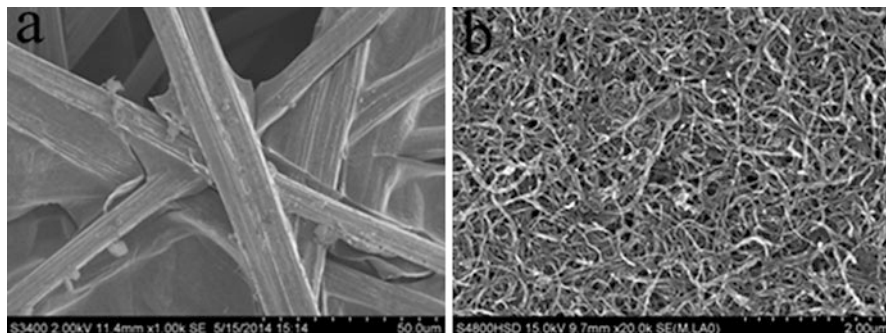


Fig. 7.3 Morphological analyses. (a) Carbon paper and (b) carbon nanotube paper [21]

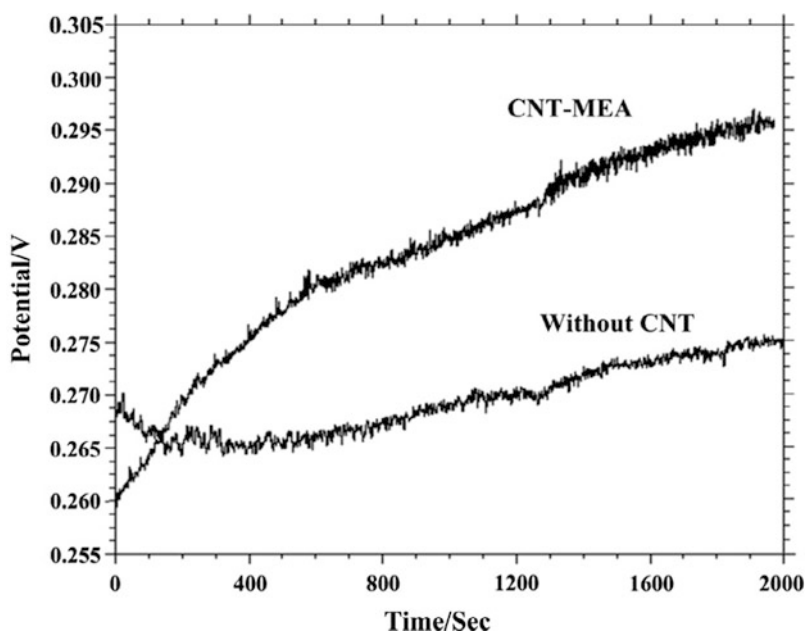


Fig. 7.4 Output potential of traditional and μ -DMFC based on CNT [20]

produces heat that aids the activity of catalyst and the water evaporation rate. The voltage of the DMFC composed of CNT-MEA is more stable within about 400 min than the DMFC composed of CP-MEA. This stability is in part due to CNT layer transport of water from GDL to the outside, which avoids flooding in GDL. The lower likelihood of flooding ensures the cathode reaction areas to remain active for longer periods. The DMFC composed of CNT-MEA produces more heat, which improves the mass transport velocity of oxygen. In spite of CNT-MEA gas blockage and limited gas penetration into GDL, the performance of the DMFC composed of CNT-MEA is superior to that of the cell composed of CP-MEA. The above gas

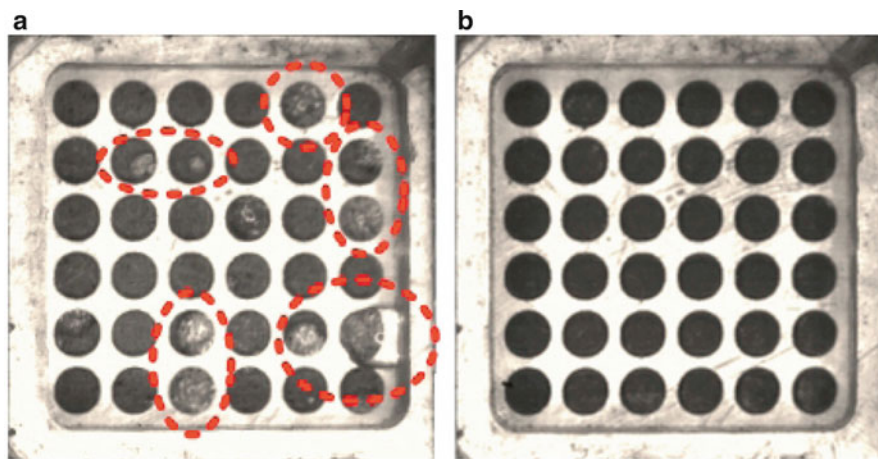


Fig. 7.5 Cathode surface of traditional and DMFC based on CNT after the long-term operation. (a) Traditional DMFC and (b) CNT-based DMFC [20]

blockage was found to dissipate in a short time. A large quantity of water is generated on the surface of GDL by chemical reaction and then condensed on the surface of the GDL in a liquid phase, during the long-term operation of the air-breathing DMFC. When the rate of water generation is higher than that of water evaporation, water will be condensed as droplets on the GDL surface which can be seen through the openings on the cathode. Flooding in the cathode prevents oxygen from entering into the GDL and decreases reaction area which leads to low efficiency and inhomogeneous distribution of oxygen mass transport in GDL, hindering performance advancement of air-breathing DMFC.

Figure 7.5 (from Deng et al., with permission License 4153540906158) shows the visual degradation of the surface phenomenon of cathode based on the voltage profile shown in Fig. 7.4. The DMFC was operated for 15 min and examined for degradation. Figure 7.5 (a) presents the cathode surface phenomenon of DMFC composed of CNT-MEA, which uses the CNT paper as water transmittal layer. Figure 7.5 (b) presents the cathode surface phenomenon of the DMFC composed of CP-MEA. We can see that the cathode surface of DMFC composed of CP-MEA has a degree of hydration (seen as droplets of water); but the DMFC composed of CNT-MEA water transmittal layer appears anhydrous at the cathode surface, which proves that using the CNT-MEA structure can prevent cathode flooding. Moreover, the unique structure of CNT paper can also enhance the efficiency of oxygen mass transport and catalyst utilization. The DMFC composed of CNT-MEA exhibits significantly higher performance than DMFC composed of CP-MEA and can operate in high methanol concentration, showing a peak power density of 23.2 mW cm^{-2} . The energy efficiency and fuel utilization efficiency are obviously improved from 11.54% to 22.7% and 36.61% to 49.34%, between MEAs composed of CP and CNTs, respectively. The water transport coefficient is 0.47 (dimensionless) from CNT-MEA, which is lower than previously reported DMFC composed of CP-MEA.

7.3 Graphene Applied in Direct Methanol Fuel Cells (DMFCs)

7.3.1 Graphene Used as Barrier Layer

In this section, the authors discuss the development of a novel anode mass transfer barrier layer for a DMFC to mitigate methanol crossover. The novel barrier layer was a composite material of stainless steel fiber felt (SSFF) and reduced graphene oxide (rGO), which was prepared by dipping a piece of SSFF plate into the graphene oxide solution and subsequently experiencing a reduction process. Using this composite material as dual-use anode barrier layer and current collector, respectively, a passive DMFC was fabricated and tested. The results showed that the novel barrier layer effectively increased the methanol mass transport resistance, lowering methanol crossover, and thus allowed the cell to operate at a higher methanol concentration. In addition, the cell fabricated with the novel barrier layer showed higher discharging stability and lower inner resistance at the same time when compared with a traditional cell.

In previous work, sintered stainless steel fiber felt (SSFF) was studied in a new anode structure, in which the anode diffusion layer also played an important role as a current collector [23]. To improve current collector efficiency, reduced graphene oxide (rGO) is proposed due to graphene hydrogels' excellent electrical properties, and porosity was constructed composed of rGO and SSFF composite structure to reduce the porosity and increase current, as a novel barrier layer for DMFC. A procedure previously described in the fabrication of graphene and foam-nickel composite was adopted [24]. Briefly, GO was scattered in deionized water, using ultrasound, in order to expel any residual air out of the SSFF, and a wafer of SSFF (0.62 mm thick) was also ultrasonically vibrated. Then GO was deposited into SSFF by leaching, with $5 \text{ mol}\cdot\text{mL}^{-1}$ GO solution. The resulting SSFF-G hydrogel composite film was then immersed in vitamin C (VC) solution ($10.0 \text{ mg}\cdot\text{mL}^{-1}$) overnight and subsequently heated at 60°C for 2 h. During this process, GO sheets were reduced to generate rGO. Then the composite sheets were placed into a freeze dryer at -20°C for 48 h after a rapid freezing by immersion in liquid nitrogen.

After the rGO-SSFF composite was generated, it was evaluated as an anode gas diffusion backing and current collector by fabricating an MEA for a DMFC. The MEA with an active area of $1 \times 1 \text{ cm}$ was fabricated by traditional procedures. Both the anode and cathode GDEs are purchased from Johnson Matthey, Inc. Nafion 117 membrane utilized had a width of $170 \mu\text{m}$, which was sandwiched between the anode GDE and cathode GDE by 18 MP hot-pressing for 5 minutes. The methanol capacity of both the new cell (SSFF-rGO) and the conventional cell was 2 mL whose performance was compared and contrasted to each other [25]. After testing the FC performance, the internal morphology of the obtained SSFF-rGO was evaluated using scanning electron microscope (SEM) and structural modifications compared with a piece of unprocessed SSFF. The SSFF-rGO performance under different methanol concentrations was also evaluated.

The physical picture of SSFF-rGO produced using the above procedure is shown in Fig. 7.6a (from Zhang et al., with permission License 4153541289218 [25]). The

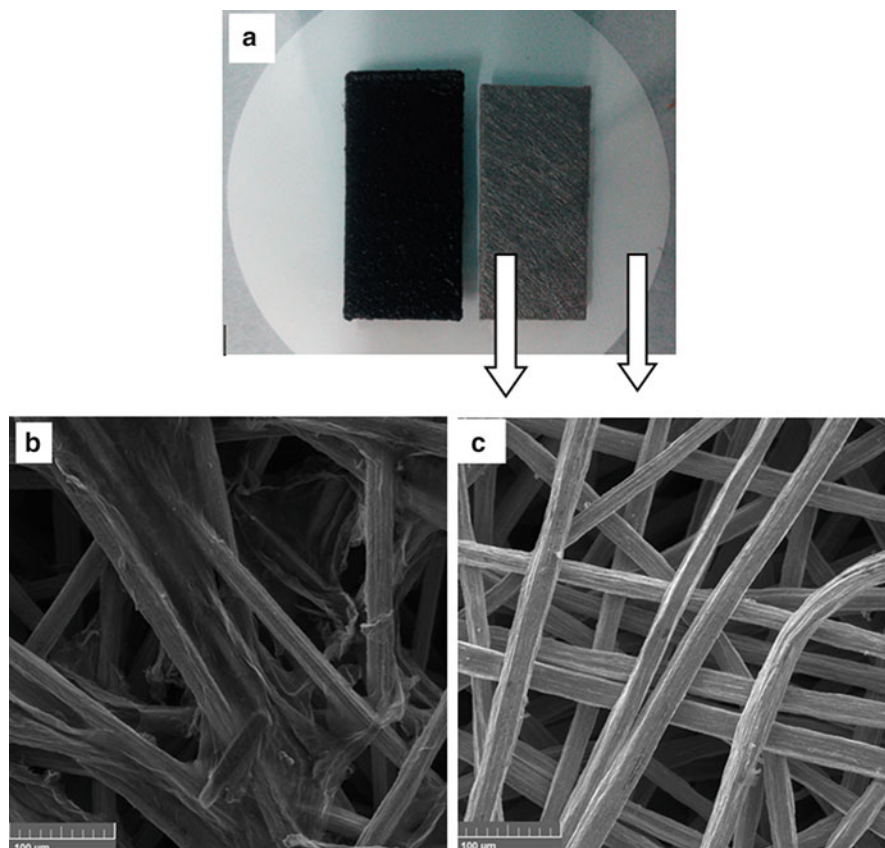


Fig. 7.6 Photograph of the (a) SSFF-rGO and SSFF, SEM of the (b) SSFF-rGO and (c) SSFF [25]

micrograph indicates that the graphene hydrogels successfully covered the surface of SSFF. The scanning electron micrographs of the SSFF-rGO composite are shown in Fig. 7.6b, c. The SEM image of SSFF-rGO (Fig. 7.6b) shows that graphene has been successfully deposited in the micropores of the whole SSFF (Fig. 7.6c). As shown in Fig. 7.6b, the SSFF-rGO with the graphene hydrogels is distributed evenly in holes of SSFF, which can potentially hinder methanol transport. The SEM images confirm that the composite possesses uniform porous inner configuration, which makes the SSFF-rGO a suitable substitute for the mass transfer barrier layer for DMFC at high methanol concentration and also guarantees high mechanical strength and superb ductility [25].

To evaluate the stability of the two materials, the fabricated cell was discharged under a constant current density of $80 \text{ mA} \cdot \text{cm}^{-2}$ at room temperature, with the novel cell at 7 M and traditional cell at 3 M shown in Fig. 7.7 (from Zhang et al., with permission License 4153541289218) [25]. It can be seen that besides a long discharging time, the novel cell has a higher and more stable cell voltage profile

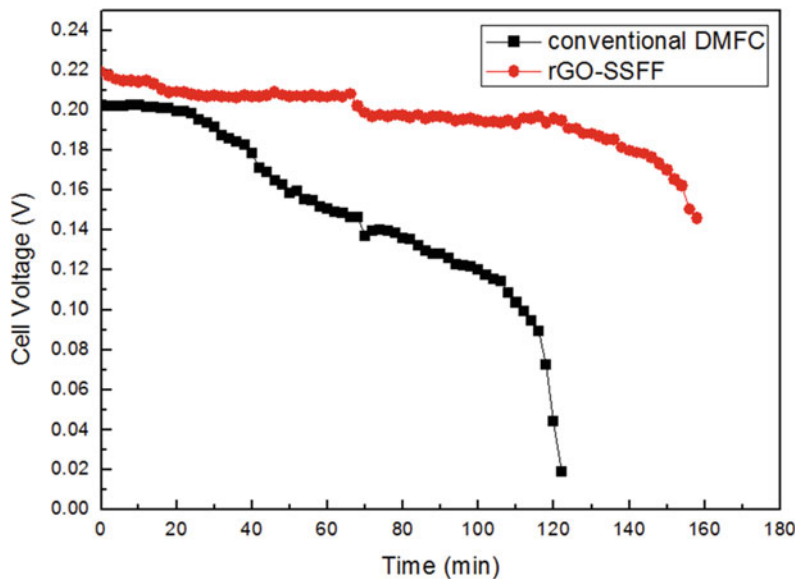


Fig. 7.7 Transient discharging curves of the μ -DMFCs under a constant current density of 80 mA cm^{-2} at 298 K [25]

compared with conventional DMFC. The differences between discharging results demonstrate and confirm the ability of the rGO-SSFF material in reducing methanol crossover under high concentration condition by taking advantages of its internal porous structure.

7.3.2 Graphene Used in Catalyst

As MEA is the core of PEMFC, the catalyst layer is the core of MEA, which makes it a significant parameter in evaluating the output performance of PEMFC. The current low efficiency, poor stability, and high cost of the catalyst remain as the biggest hurdles for the commercialization of PEMFC. In order to maintain high catalytic activity and good stability, metal particles are usually dispersed onto a support material. The catalyst support material not only determines the dispersion of metal nanoparticles but also interacts with metal particles, which in turn affects the activity and stability of the catalyst [26]. Catalyst support used in PEMFC should have the following characteristics:

1. High specific surface area, which would enhance the dispersion of metal nanoparticles and improve the catalyst surface utilization
2. Excellent conductivity that can quickly transfer the electrons of electrode reaction
3. Reasonable pore structure, which makes rapid transfer and diffusion of reactants and products

4. Strong corrosion resistance, to prevent catalyst performance in the electrolyte from rapid degradation

In summary, the most suitable material for PEMFC catalyst support currently is carbon. Graphene, an intriguing member of the carbon material family, was discovered in 2004 [27] and is a possible replacement for carbon as a structural support material. With its unique two-dimensional, single-atom layer thickness structure, graphene exhibits a large theoretical specific surface area (up to $2600 \text{ m}^2 \text{ g}^{-1}$), high electrical conductivity, high thermal conductivity, and excellent mechanical properties. In addition, chemically transformed graphene has an interlayer structure containing lattice defects (vacancies, holes) and surface functional groups (carboxyl, epoxy, and hydroxyl) that can anchor metal particles on their surface. This strong interaction between the metal and the substrate can improve the stability of the nanocatalyst [28, 29]. Fampiou et al. [28] used density functional theory (DFT) and bond-order potential calculations to prove that the defects of the surface of graphene can be a strong confinement trap of Pt nanoclusters, making Pt-graphene hybrid show excellent long-term stability. Besides, the charge transfer between the catalyst and the graphene substrate increases, and the catalytic activity of the catalyst is enhanced. Therefore, much work has been done to investigate the issue, and experiment results show graphene-based catalysts have better catalytic activity and stability than their traditional counterparts.

7.3.2.1 Graphene-Supported Catalyst for Methanol Oxidation Reaction (MOR)

Direct methanol fuel cell plays a dominant role in all kinds of P. Its fuel, methanol, has a low molecular weight, high energy density, and simple structure, which makes it one of the most suitable fuels of all kinds.

Platinum/Graphene Catalyst

Although other metal-based and nonmetal catalysts have been discovered and studied, platinum (Pt)-based catalyst still remains one of the most widely used species due to their high Pt activity toward methanol. There are three general methods to prepare Pt-based graphene hybrid. One is a chemical reduction [30–32]. Herein, Pt or other metal precursors, such as hexachloroplatinic acid (H_2PtCl_6), ruthenium (III), and chloride (RuCl_3), are mixed with graphene or GO. Then reductants, such as hydrazine hydrate (N_2H_4), sodium borohydride (NaBH_4), or hydroiodic acid (HI), are carefully added to the mixture. The reduction reaction will take place either at room temperature or at higher temperatures, depending on the chemical reductant utilized. The reduced sample is then filtered, washed, and dried under vacuum, yielding the catalyst sample which is applied on DMFC. The second method is electrodeposition [33, 34]. By applying cyclic voltammetry (CV), square wave scanning, chronoamperometry, and other electrochemical methods to electrolyte solution of precursors, the corresponding catalyst can be obtained. Potential, current density, and deposition time are parameters to control the synthesis procedure. However, the particles prepared by

electrodeposition are large, and using this method, it is difficult to fabricate materials on a large scale. The third method is microwave-assisted synthesis [35–37]. Here, the new catalyst preparation method has the advantages of simplicity, short preparation period, simple reaction control, and uniformity of the produced particles. Microwave irradiation can generate homogeneous and rapid heating of the reaction mixture that can take from seconds to one minute of reaction time. In addition, the microwave heating technique can also promote the formation of a large number of initial nuclei in the reaction, generating synthesized nanoparticles that exhibit uniform and small diameters.

Among the three synthesis methods, microwave-assisted heating with ethylene glycol (EG) method is the widely used technique [37]. Herein, a certain amount of GO is dispersed uniformly into the mixture of ethylene glycol ($C_2H_6O_2$) and isopropyl alcohol (C_3H_8O) with the ratio of 4:1 v/v using ultrasound dispersion. The chloroplatinic acid-ethylene glycol (H_2PtCl_6 -EG “ink”) solution is added and stirred for 3 h. The pH value of the ink is adjusted by sodium hydroxide (NaOH) generating an alkaline NaOH-EG solution through drop-by-drop addition until pH of the ink is >7 . Using 1 M NaOH, this corresponds approximately to the addition of 12 drops of the base. To the ink argon (Ar), gas is fed to expel (O_2) oxygen. The oxygen-depleted ink is microwave heated between 1 and 3 minutes. After cooling down to room temperature, dilute nitric acid (HNO_3) solution was added to the mixture to adjust pH value to 4. The mixture was continually stirred for 12 h, and then the product was washed repeatedly with ultrapure water until no chloride anion (Cl^-) was detected. A solid catalyst was generated after the drying process.

During the preparation of the catalyst, aggregation between GO sheets by van der Waals forces can decrease the high intrinsic specific area of graphene and thus limit the enhancement of catalytic activity. To reduce the degree of aggregation, polymers, such as poly(diallyl dimethyl ammonium) chloride (PDDA) [38, 39], chitosan [40], and N-acetylcholine (N-ACh) [41], have been used to modify graphene nano-sheets. Experimental results show that the functionalized graphene sheets have excellent efficiency and increased dispersion of noble metal nanoparticles. In our previous work, aniline ($C_6H_5NH_2$) was utilized to form nitrogen-doped carbon layer (NCL) to prevent the aggregation among graphene nano-sheets [42]. Typically, aniline monomers in 0.5 M H_2SO_4 were added to the GO solution and stirred for 3 h. The GO was subsequently reduced by sodium borohydride (rGO). The above solution was further mixed with ammonium persulfate (APS, $(NH_4)_2S_2O_8$), and polymerization was then carried out for 20 h at room temperature. Afterward, the sample was filtered and dried, and the resulting product was heat treated under 500 °C with argon gas flow for 3 h. The Pt nanoparticles were dispersed onto the composite obtained above via chemical reduction by sodium borohydride. The catalyst prepared was denoted as Pt/NCL-rGO. Figure 7.8 (from Zhang et al., with permission License 4153550310970) [42] shows transmission electron microscope (TEM) images of the synthesized Pt/NCL-rGO and Pt/rGO composite catalysts. The distribution of Pt nanoparticles on the NCL-rGO was more uniform than that on rGO. The electrochemical surface area (ECSA) of the Pt/NCL-rGO estimated by the cyclic voltammetry (CV) curves obtained in 0.5 M sulfuric acid (H_2SO_4) was $58.72 \text{ m}^2 \text{ g}^{-1}$, which was larger than

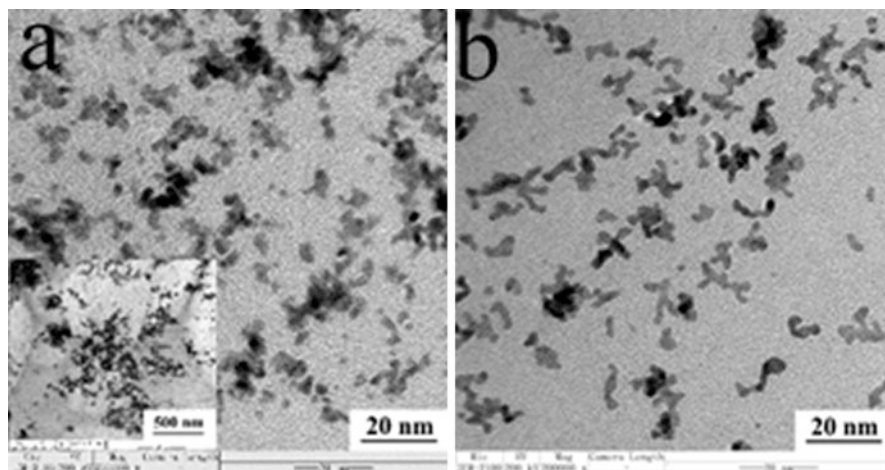


Fig. 7.8 TEM images of (a) Pt/NCL-rGO and (b) Pt/rGO [42]

the ECSA for Pt/rGO. These results were further confirmed by generating corresponding CV curves for methanol oxidation (MOR) and are shown in Fig. 7.9 (from Zhang et al., with permission License 4153550310970) [42]. Both curves have two oxidation peaks. The one located at 0.2 volts (V) in the positive scanning direction is for MOR, and the other located at 0 V in the negative direction is for the oxidation of intermediate product(s). It can be seen that the peak current density of Pt/NCL-rGO is almost twice that of Pt/rGOs. The greater ECSA of the Pt/NCL-rGO catalyst indicates better dispersal of Pt nanoparticles into the NCL-rGO layer exhibiting higher electrocatalytic activity than in the Pt/rGO catalyst layer.

Binary Pt-Based/Graphene Catalyst

The MOR process involves the adsorption of methanol and subsequent dissociation into adsorbed intermediates such as adsorbed carbon monoxide (CO_{ads}), carboxylate (COOH_{ads}), and aldehyde (CHO_{ads}) intermediary products [43]. These products will poison the Pt particles and lead to a sharp decrease of DMFC performance. To overcome this poisoning hurdle, a bifunctional mechanism has been proposed in which other metals or metal oxides are added to form the binary catalyst, which may be more tolerant to potential poisoning. So far, various binary Pt-based/graphene catalysts have been reported, and they exhibit excellent electrocatalytic activity for MOR, such as Pt-ruthenium (Ru)/graphene [44, 45], Pt-palladium (Pd)/graphene [46, 47], Pt-nickel (Ni)/graphene [48, 49], Pt-iron (Fe)/graphene [50], and Pt-tin (Sn)/graphene [51]. Ruthenium is the most widely used co-metal in commercial catalysts. Dong et al. [44] used EG reduction method and dispersed Pt particles and Ru particles onto graphene sheets. Their as-obtained catalyst showed better efficiency and activity than the commercial Pt-Ru/Vulcan XC-72R, the catalyst used in DMFC.

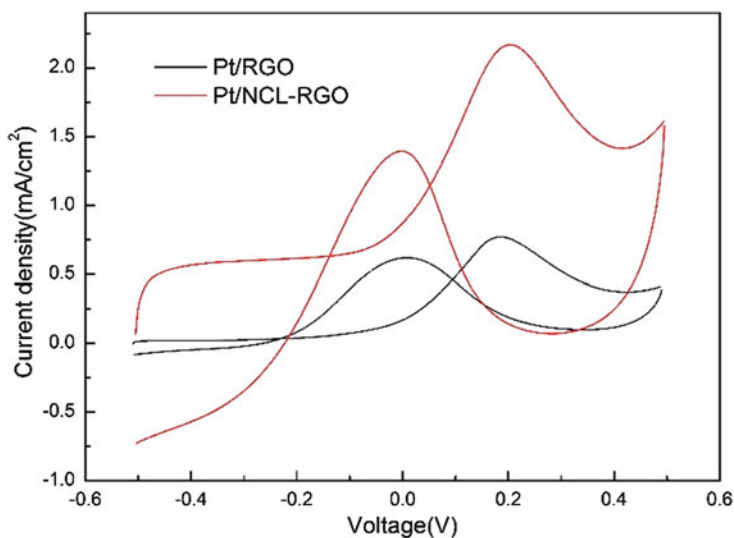


Fig. 7.9 CV curves of Pt/NCL-rGO and Pt/rGO in 0.5 M H₂SO₄ and 0.5 M methanol [42]

Among those widely used metal oxides, the rare earth cerium oxide (Ce_xO_y) attracted considerable interest because of its fluorite structure whose action (where $x = 2$ and $y = 3$ corresponding to +3 and $x = 1$ and $y = 2$ corresponding to +4 oxidation states for Ce, respectively) added advantage of Ce acting as an oxygen buffer [52]. We prepared Pt nanoparticles on the cerium (IV) oxide (CeO₂)-graphene composites by a fast and efficient one-step microwave-assisted EG method [37]. In the method, EG is regarded as a reducing agent for the metal salt compounds and a protecting agent for the metal nanoparticles. Pt/graphene was also prepared for comparison. Figure 7.10 (from Zhang et al., with permission License 4153550689598) shows the TEM images of Pt/graphene and Pt/CeO₂-graphene. Compared with Fig. 7.10b, the sizes of platinum particles, shown in Fig. 7.10a, become smaller and are better dispersed on graphene support owing to ceria incorporation. High-resolution (HR) TEM analyses suggest that the reduced Pt particles have successfully adhered to the ceria particles deposited onto the graphene sheets. Figure 7.11 (from Zhang et al., with permission License 4153550689598) [37] images demonstrate electrochemical evaluation of the Pt/CeO₂-graphene and Pt/graphene catalysts. The CV curves reveal that the former has a larger ECSA and better activity toward methanol electrooxidation than the latter catalyst. This improved catalysis is due to facile desorption of the CO_{ads} electro-oxides from the catalyst surface due to the effect of CeO₂ as a co-catalyst and oxygen storage material. The adsorbed hydroxyl (OH_{ads}) species on CeO₂ can transform (fully oxidize) CO-like poisoning species to CO₂, releasing the bound active sites on Pt surface for further MOR catalysis. Figure 7.11c shows CO adsorption-oxidation curves. Compared to the Pt/graphene catalyst, the onset and the peak potentials for adsorbed carbon monoxide (CO_{ads}) oxidation on Pt/CeO₂-graphene catalyst were

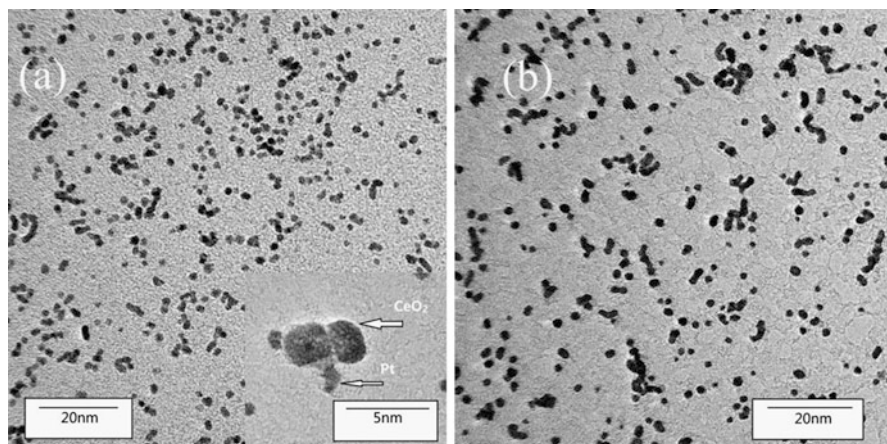


Fig. 7.10 TEM images of Pt/CeO₂-graphene (a) and Pt/graphene (b) [37]

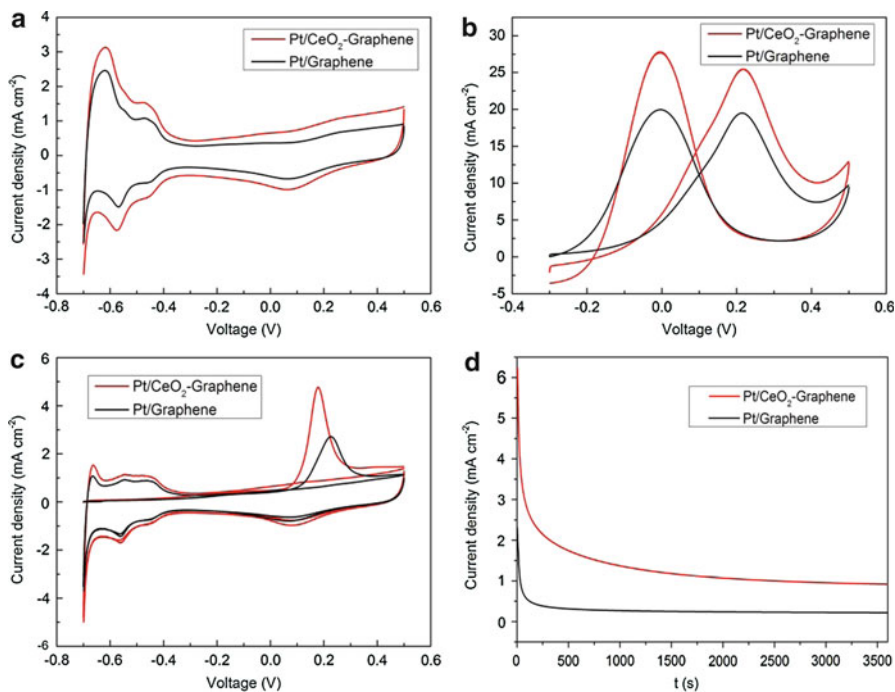


Fig. 7.11 Electrochemical properties tests. (a) CVs in 0.5 M H₂SO₄. (b) CVs in 1 M CH₃OH + 0.5 M H₂SO₄. (c) CO_{ads} stripping voltammograms. (d) Chronoamperometric curve [37]

shifted to a more negative potential, indicating that the addition of CeO₂ contributed to weakening the CO adsorptive bond on the Pt active sites. The ECSA from CO stripping voltammetry can directly reflect the CO-oxidizing ability of the catalysts,

assuming the formation of a monolayer of linearly adsorbed CO and the Columbia charge required for oxidation of CO_{ads} to be $484 \mu\text{C cm}^{-2}$. The calculated ECSA for the two catalysts were $16.3 \text{ m}^2 \text{ g}^{-1}$ and $11.4 \text{ m}^2 \text{ g}^{-1}$, respectively, by using the CO_{ads} oxidation charge after subtracting the background current, which implies that CeO_2 -metal oxide can improve catalytic activity for CO_{ads} electrooxidation. Figure 7.11d shows typical current density-time responses for MOR measured at a fixed potential of 1.02 V. The Pt/ CeO_2 -graphene catalyst shows better stability than its non-metal oxide counterpart.

Non-Pt-Based/Graphene Catalyst

As one of the most expensive noble metals, the high cost and short storage of Pt impede the full commercialization of DMFC. To solve this problem, researchers used other metal particles as substitutes for Pt, among which Pd, which is either replaced or alloyed with other noble metals such as gold (Au) and silver (Ag) and the composite catalyst used for MOR process. Palladium (Pd) is one of the most promising alternatives to Pt, due to its similar physical and electrical properties but with the added advantage of lower procurement cost. The Pd-based catalyst in the anode of DMFC reveals stronger resistance to CO poisoning. The preparation of Pd-based/graphene is similar to Pt/graphene. The modification of graphene and bifunctional mechanism also helps to boost the activity and stability of Pd-based/graphene catalyst. The electrochemical test results suggest that Pd-based/graphene catalyst possesses better catalytic performance and durability than traditional carbon materials supported Pd nanoparticles [53, 54].

In recent years, Au- and Ag-based/graphene catalysts also have attracted increasing attention [55–58] due to lower cost of usage, but with similar physical and electrical properties. The most common preparation process is a chemical reduction of metal precursors in the presence of graphene or GO. Goncalves et al. [58] used a simple chemical method in an aqueous medium and successfully prepared Au/graphene. It should be noted that no Au particles can be formed on totally reduced graphene nano-sheets since the oxygen functionalities at the graphene sheets provide reactive sites for the nucleation and growth of Au nanoparticles.

7.3.2.2 Graphene-Supported Catalyst for Hydrogen Oxidation Reaction (HOR)

Proton exchange membrane fuel cells with hydrogen as a fuel have the advantages of high energy density and zero emission and generation of water as a by-product. The FCs are widely applied in large devices such as cars; however, the widespread usage is hampered by availability, access, and storage of hydrogen, as well as the size (dimensions and mass) of the onboard PEMFC system.

Platinum-based catalysts have the highest performance for HOR with low mass fuels, due to the lower redox potential. Since the kinetics of hydrogen oxidation is more facile than the corresponding ORR, the kinetics of the HOR are usually faster at lower potentials than for the ORR, reflecting the lower Pt load (mass % of the catalyst) at the anode in PEMFC. Different types of carbon materials have been studied as the support materials for the HOR to further lower Pt load on the anode

catalyst [59]. In a pure hydrogen atmosphere, Pt/carbon black shows similar electrocatalytic activities for HOR to either Pt-Ru/carbon black or Pt/graphene in spite of the addition of Ru and the difference of supporting materials. However, at the PEMFC front-end hydrogen fuel supply is obtained through hydrogen generators, such as methanol reformer, which also produce carbon monoxide at low parts-per-million concentrations. Therefore, catalyst tolerance to CO is an essential factor in evaluating catalyst performance for the HOR. Incorporation of the sub-nano-dimension of Pt clusters supported on graphene reported by Yoo et al. exhibited better CO tolerance than the catalyst supported on carbon black [60]. The activity of the former catalyst for HOR was determined to be 52% in the presence of H₂ and 11% with H₂ containing 500 ppm of CO.

7.3.2.3 Graphene-Supported Catalyst for Oxygen Reduction Reaction (ORR)

The ORR, which takes place at the cathode of PEMFC, has a slow electrochemical kinetics compared to HOR, due to the higher potential load requirement, necessitating higher Pt catalyst loading. Therefore, fabrication of a high-efficiency catalyst for the ORR at lower Pt loading is essential for wide-scale commercialization of an FC, providing similar FC performance can be obtained to FCs using current Pt loading of 0.4 mg·Pt. The ORR is different from the MOR and HOR, in that the mechanism of catalysis can proceed by two reaction pathways depending on the reaction conditions. One is the four-electron reduction of O₂ to water as the end product ($O_2 + 4H^+ + 4e^- \rightarrow 2H_2O$) and the other is a two-step, two-electron reduction procedure, involving the formation of H₂O₂ as an intermediate ($O_2 + 4H^+ + 2e^- \rightarrow H_2O_2 + 2H^+ + 2e^- \rightarrow 2H_2O$) [61]. The former reaction pathway is more efficient than the latter one.

Like all the other reactions in PEMFC and DMFC, Pt-based catalysis requires the highest Pt load for viable activity for the ORR, and current investigators are focused on reducing the Pt loading without reducing catalytic efficiency, through either use of new forms of structural support materials or lower Pt as composite materials (coating with metals oxides, forming composite alloys, hollow shells using sacrificial Si, or as two- or three-dimensional structures are examples of how the Pt loading could be reduced without reducing the Pt catalytic efficiency for the ORR). Kou et al. [62] found that Pt nanoparticles supported on the functionalized graphene sheets exhibit larger ECSA, higher ORR activity, and enhanced stability in acid solution compared to the commercial Pt/C catalyst. Their research gave additional evidence that graphene sheets could enhance the performance of Pt catalyst at lower Pt loading than in a conventional Pt/C FC. The Pt/graphene support for ORR faces technical challenge of high cost and low durability due to the methanol crossover. The Pt alloys/graphene and other metal-based catalysts such as Pd/graphene have been fabricated as catalysts for ORR [63–66]. Yue et al. [64] found that Pt-cobalt (Co)/graphene exhibited higher ORR catalytic activity than pure Pt in alkaline solutions. Zhang et al. [65] dispersed the acid-treated Pt-Ni alloy on graphene and found that Pt-Ni/graphene had higher ORR activity than that of pure Pt catalysts in both acidic

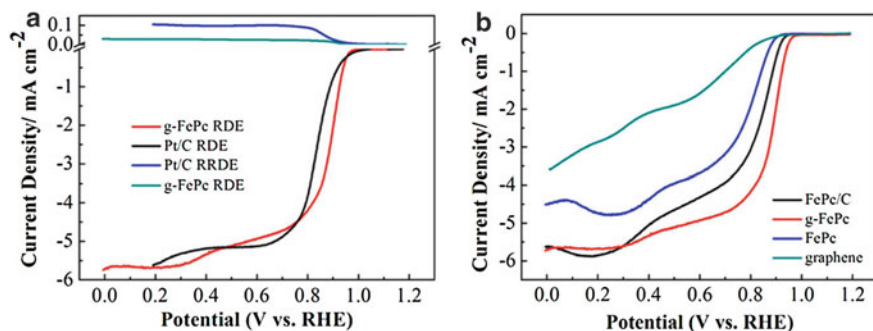


Fig. 7.12 (a) RDE and RRDE measurements of ORR at FePc/G and Pt/C catalyst in O_2 -saturated 0.1 M KOH. The ring electrode is polarized at 0.5 V (vs Ag/AgCl) with a rotation rate of 1600 rpm and a potential scan rate of 10 mV/s. (b) Comparison of the RDE polarization curves of FePc, graphene, FePc/G, and FePc supported on carbon (FePc/C) in O_2 -saturated 0.1 M KOH at 1600 rpm [72]

and alkaline solutions. Liu et al. [66] synthesized Pd-Ag nano-rings supported on graphene nano-sheets (Pd-Ag/GNs) and studied their ORR performance under alkaline circumstances. The Pd-Ag/GNs not only showed higher ORR catalytic performance but also revealed higher methanol tolerance when compared to Pd/C and Pt/C catalysts, respectively. Unlike the MOR or HOR, non-noble metal-based catalysts for use in ORR are a second major area of focus by investigators [67–70]. Among them, iron (Fe) or cobalt (Co) metal (M) incorporated onto nitrogen-doped (N) carbon (C) [M-N-C] catalysts is one promising class of cathode-supported catalyst [71]. Byon et al. [69] prepared Fe-based catalyst on rGO (Fe-N-rGO), in which the dopant nitrogen was derived from pyridine (C_5H_5N). The Fe-N-rGO exhibited higher ORR mass activity and improved stability than the Fe-N-C catalysts prepared from carbon black (CB) or oxidized CB in acid solution. Jiang et al. [72] modified graphene with iron phthalocyanine ($C_{32}H_{16}FeN_8$, FePc/G) through π - π interaction. The as-obtained FePc/G was studied as a catalyst for ORR in alkaline solution. Figure 7.12 demonstrates rotating disk electrode (RDE) and rotating ring-disk electrode (RRDE) measurements of ORR at FePc/G and Pt/C catalyst in O_2 -saturated 0.1 M KOH. The electrochemical results indicate that the graphene support can significantly improve the ORR performance of the FePc catalyst, and the FePc has a better ORR activity than the carbon-supported FePc catalyst (FePc/C).

Recently, researchers found out that N-doped graphene itself can serve as ORR catalyst without any metal particles involved [73–75]. Geng et al. [76] prepared N-doped graphene with different content of three types of nitrogen at different temperatures. It was found that the optimum temperature was 900 °C. The resulting catalyst had a very high ORR activity through a four-electron transfer process in O_2 -saturated 0.1 M KOH.

7.4 Other Nanomaterials Applied in PEMFC

Apart from carbon nanotubes (CNT) and graphene, there are other nanomaterials applied in DMFC and PEMFC. The research mainly focused on the metal catalyst supported on CNTs or graphene structured as dimensional surfaces summarized in the next sections.

7.4.1 Zero-Dimensional Nanomaterials

In the past few years, stabilizing Pt nanoparticle clusters through forming zero-dimension structures had attracted researcher as potential low-loading Pt catalyst for PEMFC applications. The clusters stabilizing Pt nanoparticles are formed in order to maximize the active number of surface versus the inactive number of Pt atoms. Bimetallic clusters have also been investigated, not only to enhance CO tolerance of catalyst but also to decrease the Pt loading. By optimizing the synthetic conditions, a very thin surface layer of Pt can be generated [77]. Chen et al. [78] reported the synthesis of a Co-Pt catalyst with a hollow sphere structure via a simple thermolytic procedure (Fig. 7.13). The as-fabricated catalyst performance was compared with Pt nanoparticle and Co-Pt nanoparticles, respectively. The Co-Pt catalyst was generated in the form of hollow spheres which exhibited a superior electrocatalytic activity toward the MOR at the same Pt loading as the Pt catalyst.

Graphene quantum dot (GQD) has been used as a new zero-dimensional (0-D) nanomaterial and has become a promising nanomaterial for fuel cell applications, due to its excellent characteristics, such as high electrical conductivity, high surface area, tunable photoluminescence, and excellent dispersion in various solvents [79–82]. Recently, Hasanzadeh et al. reported a novel nano-catalyst based on graphene quantum dot functionalized by chitosan (GQD-CS) and β -cyclodextrin (GQD- β -CD) toward MOR in alkaline solution.

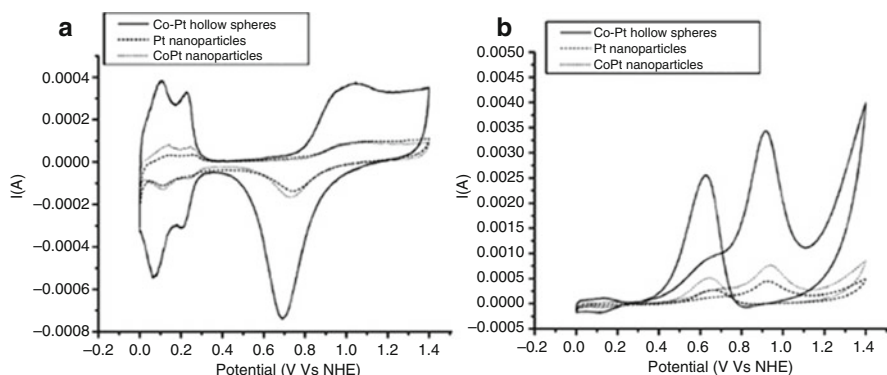


Fig. 7.13 (a) CVs of Co-Pt hollow spheres, Co-Pt nanoparticles, and Pt nanoparticles in a 0.5 M H_2SO_4 solution; (b) CVs of Co-Pt hollow spheres, Co-Pt nanoparticles, and Pt nanoparticles in a 0.5 M H_2SO_4 solution + 1 M methanol solution [78]

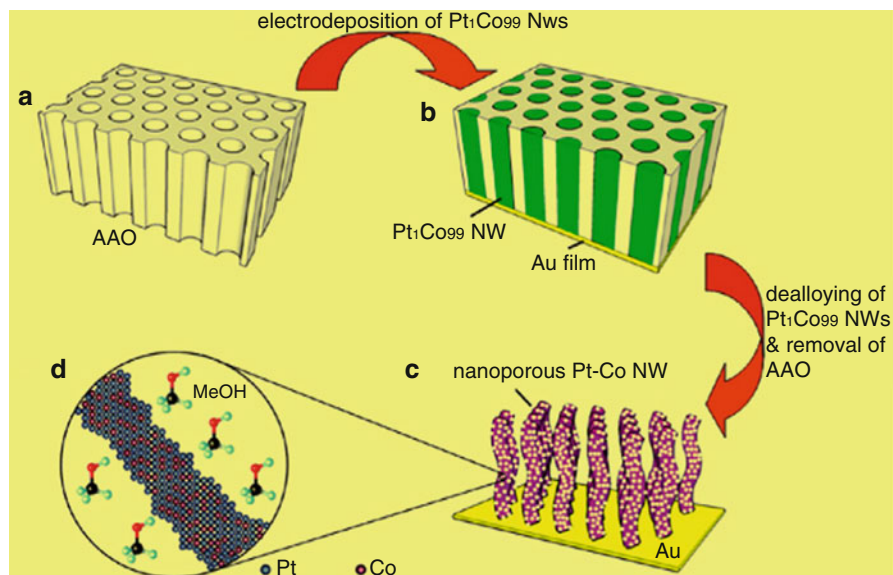


Fig. 7.14 (a–c) The schematic diagram explains the nano-porous Pt-Co nanowire fabrication process; (d) enlarged view of the ligaments [85]

7.4.2 One-Dimensional Nanomaterials

One-dimensional (1-D) nanomaterials which form the basis of higher-dimensional materials have been extensively studied. Apart from CNT, researchers have also applied nanowires, nanorods, and nano-belts in the 1-D catalyst for PEMFC, [83, 84]. Ksar et al. [83] synthesized Pd nanowires in a hexagonal mesosphere via electron beam irradiation, which showed superior electrocatalytic activity and stability for ethanol oxidation. Liu et al. [84] fabricated the nano-porous Pt-Co alloy nanowires by de-alloying electrodeposited Pt₁Co₉₉ nanowires in the presence of porous aluminum oxide (AO) membrane in a mild acidic medium, and electrochemical tests were conducted. Fig. 7.14 (from Liu et al., with permission License 501290469) [84] illustrates the preparation process. However, the specific surface area of the 1-D nanomaterials was smaller than that of the two-dimensional material, which limits their further improvement of catalytic performance.

7.4.3 Two-Dimensional Nanomaterials

Two-dimensional (2-D) nanomaterials represented by graphene have shown great advantages in energy conversion and storage applications during the past few years. For example, nanostructured transition metal sulfides have been explored as the catalyst for HOR [85, 86]. Recently, there are several literature reports involving new classes of 2-D materials being applied in PEMFC and DMFC, such as transition

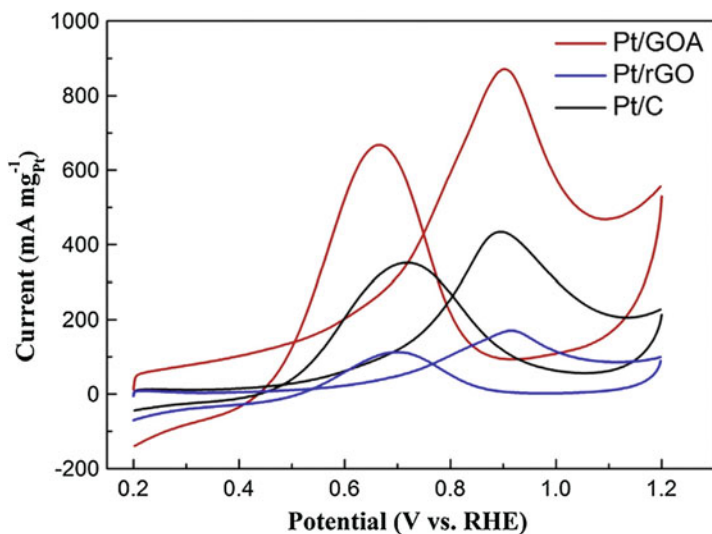


Fig. 7.15 Cyclic voltammetric curves of Pt/GOA, Pt/rGO, and commercial Pt/C in N_2 -saturated $0.5\text{ M CH}_3\text{OH} + 0.5\text{ M H}_2\text{SO}_4$ solution with a scan rate of 50 mV s^{-1}

metal compound arrays [87–89]. Due to the similarity of the electronic states to Pt at the Fermi level, group VI transition metal carbides (TMCs) exhibit catalytic properties analogous to Pt [90]. He et al. report a successful synthesis of Pt nanoparticles loaded onto the 2-D support of tantalum carbide (TaC)-nano-sheet and graphene hybrid impregnated with Pt (Pt/TaC/G) as an efficient and durable electrocatalyst for MOR. The catalyst was analyzed by X-ray photoelectron spectroscopy (XPS) and X-ray absorption spectroscopy (XAS) which indicated synergetic chemical coupling effects between the Pt and TaC/G that led to increased improvement in ORR catalytic activity and catalyst durability.

7.4.4 Three-Dimensional Nanomaterials

Two-dimensional nanomaterials have a tendency to stack during the utilization process, due to layer-to-layer interactions. To minimize stacking higher-order three-dimensional (3-D) materials have been proposed and fabricated by researchers. These nanomaterials hold unique morphologies that provide a larger surface area which enhance the transfer of reactants and products. Graphene oxide aerogel (GOA) and graphene aerogel (GA), as the 3-D constructs of graphene, have attracted significant attention [91–93]. Graphene oxide aerogel can be obtained by supercritical CO_2 drying or freeze-drying of GOA prepared by cross-linking graphene nano-sheets with multivalent metal ions or amino groups. Moreover, GA can also be prepared by supercritical CO_2 drying or freeze-drying of graphene hydrogel that is prepared by hydrothermal treatment of GO. The as-prepared GOA or GA not only

maintain the intrinsic properties of 2-D graphene sheets but also exhibit other excellent functions of GO with improved catalytic performance. Our group successfully dispersed Pt nanoparticles on GOA via chemical reduction and examined its performance as a catalyst for DMFC [94]. The prepared Pt/GOA showed a low degree of graphitization as ascertained by an analysis of XRD spectrum, indicating that the graphene sheets did not stack. The SEM images also indicated that Pt/GOA maintained excellent 3-D porous structure, which not only facilitated reaction mass transfer but also avoided the detrimental influence of reduced active surface area of Pt particles due to the stacking of the graphene sheets.

The CV results also revealed that the ECSA of Pt/GOA reached $95.5 \text{ m}^2 \cdot \text{g}^{-1}$, which was twice that of commercial Pt/C. Fig. 7.15 (from Duan et al., with permission License 501290464) [94] demonstrated the CV curves of Pt/GOA, Pt/rGO, and commercial Pt/C in N_2 -saturated $0.5 \text{ M CH}_3\text{OH} + 0.5 \text{ M H}_2\text{SO}_4$ solution. The peak current density of Pt/GOA was $876 \text{ mA} \cdot \text{mg}^{-1}_{\text{Pt}}$, which was much higher than the other two samples. The CV data demonstrate that the Pt/GOA catalyst exhibited greater electrochemical activity (ESA) than either the Pt/rGO or the Pt/C catalyst, which resulted in the higher ECSA of Pt nanoparticles on Pt/GOA due to lower layer stacking and higher area. In addition, chronoamperometric measurements indicated that the catalytic stability toward MOR was also strongly enhanced.

7.5 Conclusion

A diverse type and structuring of nanomaterials have played a significant role enabling improved performance of PEMFCs and DMFCs by researchers during the past decade. The wide application of 0-, 1-, 2-, and 3-D nanomaterials contributed to the decrease in FC cost due to lower Pt loading and increased improvement of FC performance. Yet the performance of PEMFCs and DMFCs cannot meet the expected demand through increased commercialization, due to Pt loading being the limiting factor in FC design. With the emergence and development of new nanomaterials that greatly diminish Pt loading without loss of performance, FCs with more innovative structure and lesser Pt loading are expected to lead to improved FC performance, which in turn will lower FC cost and increase availability for a variety of applications. The greater usage of PEMFCs and DMFCs will lead to reduced use of fossil fuels mitigating the negative effects of global warming and increased access to portable power to rural areas that are not electrified, benefiting rural societies.

Acknowledgment This research is financially supported by the National Natural Science Funds of China (Agreement Codes 61404037 and 61376113).

References

1. T.J. Yen, N. Fang, X. Zhang, G.Q. Lu, C.Y. Wang, A micro methanol fuel cell operating at near room temperature. *Appl. Phys. Lett.* **83**, 4056–4058 (2003)

2. C. Xu, T.S. Zhao, A new flow field design for polymer electrolyte-based fuel cells. *Electrochem. Commun.* **9**, 497–503 (2007)
3. H. Dai, H.M. Zhang, Q.T. Luo, Y. Zhang, C. Bi, Properties and fuel cell performance of proton exchange membranes prepared from disulfonated poly (sulfide sulfone). *J. Power Sources* **185**, 19–25 (2008)
4. Y.F. Zhang, P. Zhang, B. Zhang, J.M. Li, H.C. Deng, X.W. Liu, Development of an air-breathing direct methanol fuel cell with the cathode shutter current collectors. *Int. J. Hydrog. Energy* **35**, 5638–5646 (2010)
5. B. Zhang, Y.F. Zhang, H. He, J.M. Li, Z.Y. Yuan, C.R. Na, X.W. Liu, Development and performance analysis of a metallic micro-direct methanol fuel cell for high-performance applications. *J. Power Sources* **195**, 7338–7348 (2010)
6. Z. Yuan, Y. Zhang, J. Leng, Y. Gao, X. Liu, Development of a 4-cell air-breathing micro direct methanol fuel cell stack. *J. Power Sources* **202**, 134–142 (2012)
7. T.S. Zhao, C. Xu, R. Chen, W.W. Yang, Small direct methanol fuel cells with passive supply of reactants. *J. Power Sources* **191**, 185–202 (2009)
8. F. Achmad, S.K. Kamarudin, W.R.W. Daud, E.H. Majlan, Passive direct methanol fuel cells for portable electronic devices. *Appl. Energy* **88**, 1681–1689 (2011)
9. T.S. Zhao, C. Xu, R. Chen, W.W. Yang, Mass transport phenomena in direct methanol fuel cells. *Prog. Energy Combust. Sci.* **35**, 275–292 (2009)
10. R. Chen, T.S. Zhao, Porous current collectors for passive direct methanol fuel cells. *Electrochim. Acta* **52**, 4317–4324 (2007)
11. Y. Li, X.L. Zhang, L. Nie, Y.F. Zhang, X.W. Liu, Stainless steel fiber felt as cathode diffusion backing and current collector for a micro direct methanol fuel cell with low methanol crossover. *J. Power Sources* **245**, 520–528 (2014)
12. S.C. Yao, X.D. Tang, C.C. Hsieh, Y. Alyousef, M. Vladime, G.K. Fedder, C.H. Amon, Micro-electro-mechanical systems (MEMS)-based micro-scale direct methanol fuel cell development. *Energy* **31**, 636–649 (2006)
13. H. Peng, P. Chen, H. Chen, C. Chieng, T. Yeh, C. Pan, F. Tseng, Passive cathodic water/air management device for micro-direct methanol fuel cells. *J. Power Sources* **195**, 7349–7358 (2010)
14. Y.A. Zhou, X.H. Wang, X. Guo, X.P. Qiu, L.T. Liu, A water collecting and recycling structure for silicon-based micro direct methanol fuel cells. *Int. J. Hydrog. Energy* **37**, 967–976 (2012)
15. M.M.H.-S. rabadi, E. Dashtimoghadam, F.S. Majedi, S.H. Emami, H. Moaddel, A high-performance chitosan-based double layer proton exchange membrane with reduced methanol crossover. *Int. J. Hydrog. Energy* **36**, 6105–6111 (2011)
16. J. Kim, J.-D. Jeon, S.-Y. Kwak, Delamination of microporous layered silicate by acid-hydrothermal treatment and its use for reduction of methanol crossover in DMFC. *Microporous Mesoporous Mater.* **168**, 148–154 (2013)
17. H. Deligöz, S. Yilmaztürk, T. Gümüşoğlu, Improved direct methanol fuel cell performance of layer-by-layer assembled composite and catalyst containing membranes. *Electrochim. Acta* **111**, 791–796 (2013)
18. Y. Xue, S. Chan, Layer-by-layer self-assembly of CHI/PVS-Nafion composite membrane for reduced methanol crossover and enhanced DMFC performance. *Int. J. Hydrog. Energy* **40**, 1877–1885 (2015)
19. Y.-C. Park, D.-H. Kim, S. Lim, S.-K.Y. Kim, D.-H. Peck, D.-H. Jung, Design of a MEA with multi-layer electrodes for high concentration methanol DMFCs. *Int. J. Hydrog. Energy* **37**, 4717–4727 (2012)
20. H. Deng, Y. Zhang, Z. Xue, L. Yang, X. Zhang, X. Liu, A CNT (carbon nanotube) paper as cathode gas diffusion electrode for water management of passive μ -DMFC (micro-direct methanol fuel cell) with highly concentrated methanol. *Energy* **82**, 236–241 (2015)
21. H. Deng, Y. Zhang, Y. Li, X. Zhang, X. Liu, A CNT-MEA compound structure of micro-direct methanol fuel cell for water management. *Microelectron. Eng.* **110**, 288–291 (2013)
22. S.H. Ng, J. Wang, Z.P. Guo, J. Chenb, et al., *J. Electrochim. Acta* **51**, 23 (2005)

23. R. Xue, S. Sang, H. Jin, Q. Shen, Y. Zhang, X. Liu, X. Zhang, Stainless steel fiber felt as the anode diffusion backing and current collector for μ -DMFC. *Microelectron. Eng.* **119**, 159–163 (2014)
24. S. Ye, F. Jiachun, W. Peiyi, Deposition of three-dimensional graphene aerogel on nickel foam as a binder-free supercapacitor electrode. *ACS Appl. Mater. Interfaces* **5**, 7122–7129 (2013)
25. Y. Zhang, R. Xue, X. Zhang, J. Song, X. Liu, rGO deposited in stainless steel fiber felt as mass transfer barrier layer for μ -DMFC. *Energy* **91**, 1081–1086 (2015)
26. J. Rajeswari, B. Viswanathan, Tungsten trioxide nanorods as supports for platinum in methanol oxidation. *Mater. Chem. Phys.* **106**(2–3), 168–174 (2007)
27. K.S. Novoselov, A.K. Geim, S.V. Morozov, D. Jiang, Y. Zhang, S.V. Dubonos, A.A. Firsov, Materials and methods: Electric field effect in atomically thin carbon films. *Science* **306**(5696), 666–669 (2004)
28. I. Fampiou, A. Ramasubramaniam, Binding of Pt nanoclusters to point defects in graphene: Adsorption, morphology, and electronic structure. *J. Phys. Chem. C* **116**(11), 6543–6555 (2012)
29. R. Kou, Y. Shao, D. Mei, Z. Nie, D. Wang, C. Wang, et al., Stabilization of electrocatalytic metal nanoparticles at metal-metal oxide-graphene triple junction points. *J. Am. Chem. Soc.* **133**(8), 2541–2547 (2011)
30. C. Huang, C. Li, G. Shi, Graphene based catalysts. *Energy Environ. Sci.* **5**(10), 8848–8868 (2012)
31. B. Seger, P.V. Kamat, Electrocatalytically active graphene-platinum nanocomposites. Role of 2-d carbon support in PEM fuel cells. *J. Phys. Chem. C* **113**(19), 7990–7995 (2009)
32. R.I. Jafri, T. Arockiadoss, N. Rajalakshmi, S. Ramaprabhu, Nanostructured Pt dispersed on graphene-multiwalled carbon nanotube hybrid nanomaterials as electrocatalyst for PEMFC. *J. Electrochem. Soc.* **157**(6), B874 (2010)
33. H. Meng, C. Wang, P.K. Shen, G. Wu, Palladium thorn clusters as catalysts for electrooxidation of formic acid. *Energy Environ. Sci.* **4**(4), 1522–1526 (2011)
34. Y.G. Zhou, J.J. Chen, F.B. Wang, Z.H. Sheng, X.H. Xia, A facile approach to the synthesis of highly electroactive Pt nanoparticles on graphene as an anode catalyst for direct methanol fuel cells. *Chem. Commun.* **46**(32), 5951–5953 (2010)
35. S. Sharma, A. Ganguly, P. Papakonstantinou, X. Miao, M. Li, J.L. Hutchison, et al., Rapid microwave synthesis of CO tolerant reduced graphene oxide-supported platinum electrocatalysts for oxidation of methanol. *J. Phys. Chem. C* **114**(45), 19459–19466 (2010)
36. P. Kundu, C. Nethravathi, P.A. Deshpande, M. Rajamathi, G. Madras, N. Ravishankar, Ultrafast microwave-assisted route to surfactant-free ultrafine Pt nanoparticles on graphene: Synergistic co-reduction mechanism and high catalytic activity. *Chem. Mater.* **23**(11), 2772 (2011)
37. H. Chen, J. Duan, X. Zhang, Y. Zhang, C. Guo, L. Nie, et al., One step synthesis of Pt/CeO₂-graphene catalyst by microwave-assisted ethylene glycol process for direct methanol fuel cell. *Mater. Lett.* **126**, 9–12 (2014)
38. Z. Wang, J. Xia, X. Guo, Y. Xia, S. Yao, F. Zhang, et al., Platinum/graphene functionalized by PDDA as a novel enzyme carrier for hydrogen peroxide biosensor. *Anal. Methods* **5**(2), 483–488 (2012)
39. J.D. Qiu, G.C. Wang, R.P. Liang, X.H. Xia, H.W. Yu, Controllable deposition of platinum nanoparticles on graphene as an electrocatalyst for direct methanol fuel cells. *J. Phys. Chem. C* **115**(31), 15639–15645 (2011)
40. Z. Cui, C.M. Li, S.P. Jiang, PtRu catalysts supported on heteropolyacid and chitosan functionalized carbon nanotubes for methanol oxidation reaction of fuel cells. *Phys. Chem. Chem. Phys.* **13**(36), 16349 (2011)
41. J. Duan, X. Liu, H. Chen, Y. Zhang, J. Du, X. Zhang, Poly(n-acetylaniline) functionalized graphene nanosheets supported Pt electrocatalysts for methanol oxidation. *Microelectron. Eng.* **121**(4), 100–103 (2014)
42. X. Zhang, W. Yuan, J. Duan, Y. Zhang, X. Liu, Graphene nanosheets modified by nitrogen-doped carbon layer to support Pt nanoparticles for direct methanol fuel cell. *Microelectron. Eng.* **141**, 234–237 (2015)

43. J.M. Léger, Mechanism aspects of methanol oxidation on platinum-based electrocatalysts. *J. Appl. Electrochem.* **31**, 767–771 (2001)
44. L. Dong, R.R.S. Gari, Z. Li, M.M. Craig, S. Hou, Graphene-supported platinum and platinum–ruthenium nanoparticles with high electrocatalytic activity for methanol and ethanol oxidation. *Carbon* **48**(3), 781–787 (2010)
45. H. Li, X. Zhang, H. Pang, C. Huang, J. Chen, PMo12-functionalized graphene nanosheet-supported PtRu nanocatalysts for methanol electro-oxidation. *J. Solid State Electrochem.* **14** (12), 2267–2274 (2010)
46. H. Ji, M. Li, Y. Wang, F. Gao, Electrodeposition of graphene-supported PdPt nanoparticles with enhanced electrocatalytic activity. *Electrochem. Commun.* **24**(1), 17–20 (2012)
47. Y. Lu, Y. Jiang, H. Wu, W. Chen, Nano-PtPd cubes on graphene exhibit enhanced activity and durability in methanol electrooxidation after CO stripping–cleaning. *J. Phys. Chem. C* **117**(6), 2926–2938 (2013)
48. Y. Hu, P. Wu, Y. Yin, H. Zhang, C. Cai, Effects of structure, composition, and carbon support properties on the electrocatalytic activity of Pt–Ni–graphene nanocatalysts for the methanol oxidation. *Appl. Catal. B Environ.* **111**(6), 208–217 (2011)
49. Y. Hu, P. Wu, H. Zhang, C. Cai, Synthesis of graphene-supported hollow Pt–Ni nanocatalysts for highly active electrocatalysis toward the methanol oxidation reaction. *Electrochim. Acta* **85** (4), 314–321 (2012)
50. Z.Y. Ji, G.X. Zhu, X.P. Shen, H. Zhou, C.M. Wu, M. Wang, Reduced graphene oxide supported FePt alloy nanoparticles with high electrocatalytic performance for methanol oxidation. *New J. Chem.* **36**(9), 1774–1780 (2012)
51. F. Han, X. Wang, J. Lian, Y. Wang, The effect of Sn content on the electrocatalytic properties of Pt–Sn nanoparticles dispersed on graphene nanosheets for the methanol oxidation reaction. *Carbon* **50**(15), 5498–5504 (2012)
52. C.L. Perkins, M.A. Henderson, C.H.F. Peden, G.S. Herman, Self-diffusion in ceria. *J. Vacuum Sci. Tech. Vacuum Surfaces Films* **19**(4 PT 2), 217–218 (2001)
53. R. Awasthi, R.N. Singh, Graphene-supported Pd–Ru nanoparticles with superior methanol electrooxidation activity. *Carbon* **51**(1), 282–289 (2013)
54. P. Xi, F. Chen, G. Xie, C. Ma, H. Liu, C. Shao, et al., Surfactant free rGO/Pd nanocomposites as highly active heterogeneous catalysts for the hydrolytic dehydrogenation of ammonia borane for chemical hydrogen storage. *Nanoscale* **4**(18), 5597 (2012)
55. E.J. Lim, S.M. Choi, H.S. Min, Y. Kim, S. Lee, W.B. Kim, Highly dispersed ag nanoparticles on nanosheets of reduced graphene oxide for oxygen reduction reaction in alkaline media. *Electrochem. Commun.* **28**(1), 100–103 (2013)
56. X. Liu, X. Wang, P. He, L. Yi, Z. Liu, X. Yi, Influence of borohydride concentration on the synthesized au/graphene nanocomposites for direct borohydride fuel cell. *J. Solid State Electrochem.* **16**(12), 3929–3937 (2012)
57. S.J. Cho, A. Suri, X. Mei, J. Ouyang, In situ deposition of gold nanostructures with well-defined shapes on unfunctionalized reduced graphene oxide through chemical reduction of a dry gold precursor with ethylene glycol vapor. *RSC Adv.* **3**(3), 1201–1209 (2012)
58. G. Goncalves, P.A.A.P. Marques, C.M. Granadeiro, H.I.S. Nogueira, M.K. Singh, J. Grácio, Surface modification of graphene nanosheets with gold nanoparticles: The role of oxygen moieties at graphene surface on gold nucleation and growth. *Chem. Mater.* **21**, 4796–4802 (2009)
59. M. Carmo, V.A. Paganin, J.M. Rosolen, E.R. Gonzalez, Alternative supports for the preparation of catalysts for low-temperature fuel cells: The use of carbon nanotubes. *J. Power Sources* **142** (1), 169–176 (2005)
60. E.J. Yoo, T. Okada, T. Akita, M. Kohyama, I. Honma, J. Nakamura, Sub-nano-Pt cluster supported on graphene nanosheets for CO tolerant catalysts in polymer electrolyte fuel cells. *J. Power Sources* **196**(1), 110–115 (2011)
61. E. Yeager, Electrocatalysts for molecular oxygen reduction. *Electrochim. Acta* **29**, 1527–1537 (1984)

62. R. Kou, Y. Shao, D. Wang, M.H. Engelhard, J.H. Kwak, J. Wang, et al., Enhanced activity and stability of Pt catalysts on functionalized graphene sheets for electrocatalytic oxygen reduction. *Electrochem. Commun.* **11**(5), 954–957 (2009)
63. H.J. Kim, S.M. Choi, H.S. Min, S. Green, G.W. Huber, W.B. Kim, Efficient electrooxidation of biomass-derived glycerol over a graphene-supported PtRu electrocatalyst. *Electrochem. Commun.* **13**(8), 890–893 (2011)
64. Q. Yue, K. Zhang, X. Chen, L. Wang, J. Zhao, J. Liu, J. Jia, Generation of OH radicals in oxygen reduction reaction at Pt–Co nanoparticles supported on graphene in alkaline solutions. *Chem. Commun.* **46**(19), 3369–3371 (2010)
65. K. Zhang, Q. Yue, G. Chen, Y. Zhai, L. Wang, H. Wang, H. Li, Effects of acid treatment of Pt–Ni alloy nanoparticles@ graphene on the kinetics of the oxygen reduction reaction in acidic and alkaline solutions. *J. Phys. Chem. C* **115**(2), 379–389 (2010)
66. M. Liu, Y. Lu, W. Chen, Electrocatalysts: PdAg nanorings supported on graphene nanosheets: Highly methanol-tolerant cathode electrocatalyst for alkaline fuel cells (adv. Funct. Mater. 10/2013). *Adv. Funct. Mater.* **23**(23), 1348–1348 (2013)
67. Z.S. Wu, S. Yang, S. Yi, K. Parvez, X. Feng, K. Müllen, 3D nitrogen-doped graphene aerogel-supported Fe₃O₄ nanoparticles as efficient electrocatalysts for the oxygen reduction reaction. *J. Am. Chem. Soc.* **134**(22), 9082 (2012)
68. C. Zhang, R. Hao, H. Yin, F. Liu, Y. Hou, Iron phthalocyanine and nitrogen-doped graphene composite as a novel non-precious catalyst for the oxygen reduction reaction. *Nanoscale* **4**(23), 7326–7329 (2012)
69. H.R. Byon, S. Jin, S.H. Yang, Graphene-based non-noble-metal catalysts for oxygen reduction reaction in acid. *Chem. Mater.* **23**(23), 3421–3428 (2011)
70. R.J. Toh, H.L. Poh, Z. Sofer, M. Pumera, Transition metal (Mn, Fe, Co, Ni)-doped graphene hybrids for electrocatalysis. *Chem. Asian J.* **8**(6), 1295–1300 (2013)
71. M. Lefèvre, E. Proietti, F. Jaouen, Dodelet, Supporting material for: Iron-based catalysts with improved oxygen reduction activity in polymer electrolyte fuel cells. *Science* **324**(5923), 71–74 (2009)
72. Y. Jiang, Y. Lu, X. Lv, D. Han, Q. Zhang, L. Niu, et al., Enhanced catalytic performance of Pt-free iron phthalocyanine by graphene support for efficient oxygen reduction reaction. *ACS Catal.* **3**(6), 1263–1271 (2013)
73. Z. Yang, H. Nie, X. Chen, X. Chen, S. Huang, Recent progress in doped carbon nanomaterials as effective cathode catalysts for fuel cell oxygen reduction reaction. *J. Power Sources* **236**(16), 238–249 (2013)
74. C. Zhang, R. Hao, H. Liao, Y. Hou, Synthesis of amino-functionalized graphene as metal-free catalyst and exploration of the roles of various nitrogen states in oxygen reduction reaction. *Nano Energy* **2**(1), 88–97 (2013)
75. C. He, Z. Li, M. Cai, M. Cai, J.Q. Wang, Z. Tian, et al., A strategy for mass production of self-assembled nitrogen-doped graphene as catalytic materials. *J. Mater. Chem. A* **1**(4), 1401–1406 (2012)
76. D. Geng, Y. Chen, Y. Chen, Y. Li, R. Li, X. Sun, et al., High oxygen-reduction activity and durability of nitrogen-doped graphene. *Energy Environ. Sci.* **4**(3), 760–764 (2011)
77. J.B. Raoof, R. Ojani, S. Rashid-Nadimi, Electrochemical synthesis of bimetallic Au@Pt nanoparticles supported on gold film electrode by means of self-assembled monolayer. *J. Electroanal. Chem.* **641**(1–2), 71–77 (2010)
78. G. Chen, D. Xia, Z. Nie, Z. Wang, L. Wang, J. Zhang, et al., Facile synthesis of co-Pt hollow sphere electrocatalyst. *Chem. Mater.* **19**(7), 1840–1844 (2007)
79. C.S. Lim, K. Hola, A. Ambrosi, R. Zboril, M. Pumera, Graphene and carbon quantum dots electrochemistry. *Electrochem. Commun.* **52**, 75–79 (2015)
80. M. Bacon, S.J. Bradley, T. Nann, Graphene quantum dots. *Part. Part. Syst. Charact.* **31**(4), 415–428 (2014)

81. Q. Li, B.W. Noffke, Y. Liu, L.S. Li, Understanding fundamental processes in carbon materials with well-defined colloidal graphene quantum dots. *Curr. Opin. Colloid Interface Sci.* **20**(5-6), 346–353 (2015)
82. L. Lin, M. Rong, F. Luo, D. Chen, Y. Wang, X. Chen, Luminescent graphene quantum dots as new fluorescent materials for environmental and biological applications. *TrAC Trends Anal. Chem.* **54**, 83–102 (2013)
83. F. Ksar, L. Ramos, B. Keita, L. Nadjo, P. Beaunier, H. Remita, Bimetallic palladium– gold nanostructures: Application in ethanol oxidation. *Chem. Mater.* **21**(15), 3677–3683 (2009)
84. L. Liu, E. Pippel, R. Scholz, U. Gösele, Nanoporous Pt-Co alloy nanowires: Fabrication, characterization, and electrocatalytic properties. *Nano Lett.* **9**(12), 4352–4358 (2009)
85. P. Du, Y. Zhu, J. Zhang, D. Xu, W. Peng, G. Zhang, et al., Metallic 1t phase MoS₂ nanosheets as a highly efficient co-catalyst for the photocatalytic hydrogen evolution of CdS nanorods. *RSC Adv.* **6**(78), 74394–74399 (2016)
86. L.F. Zhang, G. Ou, L. Gu, Z.J. Peng, L.N. Wang, H. Wu, A highly active molybdenum multisulfide electrocatalyst for the hydrogen evolution reaction. *RSC Adv.* **6**(109), 107158–107162 (2016)
87. S. Mu, X. Chen, R. Sun, X. Liu, H. Wu, D. He, et al., Nano-size boron carbide intercalated graphene as high performance catalyst supports and electrodes for PEM fuel cells. *Carbon* **103**, 449–456 (2016)
88. P. Wu, H. Lv, T. Peng, D. He, S. Mu, Nano conductive ceramic wedged graphene composites as highly efficient metal supports for oxygen reduction. *Sci. Rep.* **4**(2), 3968 (2014)
89. X. Chen, D. He, H. Wu, X. Zhao, J. Zhang, K. Cheng, et al., Platinized graphene/ceramics nano-sandwiched architectures and electrodes with outstanding performance for PEM fuel cells. *Sci. Rep.* **5**, 16246 (2015)
90. C. He, J. Tao, Y. Ke, Y. Qiu, Graphene-supported small tungsten carbide nanocrystals promoting a Pd catalyst towards formic acid oxidation. *RSC Adv.* **5**(82), 66695–66703 (2015)
91. M. Nawaz, W. Miran, J. Jang, D.S. Lee, One-step hydrothermal synthesis of porous 3d reduced graphene oxide/TiO₂ aerogel for carbamazepine photodegradation in aqueous solution. *Appl. Catal. B Environ.* **203**, 85–95 (2017)
92. X. Jia, J. Wang, X. Zhu, T. Wang, F. Yang, W. Dong, et al., Synthesis of lightweight and flexible composite aerogel of mesoporous iron oxide threaded by carbon nanotubes for microwave absorption. *J. Alloys Compd.* **697**, 138–146 (2016)
93. X. Xu, Y. Sun, W. Qiao, X. Zhang, X. Chen, X. Song, et al., 3D MoS₂-graphene hybrid aerogels as catalyst for enhanced efficient hydrogen evolution. *Appl. Surf. Sci.* **396**(8), 1520–1527 (2017)
94. J. Duan, X. Zhang, W. Yuan, H. Chen, S. Jiang, X. Liu, et al., Graphene oxide aerogel-supported Pt electrocatalysts for methanol oxidation. *J. Power Sources* **285**, 76–79 (2015)